Biochemistry

pubs.acs.org/biochemistry Article

Elucidating the Kinetic Mechanism of Human METTL16

Kurtis Breger and Jessica A. Brown*

Cite This: *Biochemistry* 2023, 62, 494−506 Read Online

ACCESS | Metrics & More | Article Recommendations | Supporting Information

ABSTRACT: Methyltransferase-like protein 16 (METTL16) is one of four catalytically active, *S*-adenosylmethionine (SAM)-dependent m^{6}A RNA methyltransferases in humans. Well-known methylation targets of METTL16 are U6 small nuclear RNA (U6 snRNA) and the MAT2A mRNA hairpins; however, METTL16 binds to other RNAs, including the 3′ triple helix of the metastasis-associated lung adenocarcinoma transcript 1 (MALAT1). Herein, we investigated the kinetic mechanism and biochemical properties of METTL16. METTL16 is a monomer in complex with either the MALAT1 triple helix or U6 snRNA and binds to these RNAs with respective dissociation constants of 31 nM and 18 nM, whereas binding to the methylated U6 snRNA product is 1.1 μM. The MALAT1 triple helix, on the other hand, is not methylated by METTL16 under *in vitro* conditions. Using the U6 snRNA to study methylation steps, preincubation and isotope partitioning assays indicated an ordered-sequential mechanism, whereby METTL16 binds U6 snRNA before SAM. The apparent dissociation constant for the METTL16·U6 snRNA·SAM ternary complex is 126 μM. Steady-state kinetic assays established a k_{cat} of 0.07 min^{-1}, and single-turnover assays established a k_{chem} of 0.56 min^{-1}. Furthermore, the methyltransferase domain of METTL16 methylated U6 snRNA with an apparent dissociation constant of 736 μM and a k_{chem} of 0.42 min^{-1}, suggesting that the missing vertebrate conserved regions weaken the ternary complex but do not induce any rate-limiting conformational rearrangements of the U6 snRNA. This study helps us to better understand the catalytic activity of METTL16 in the context of its biological functions.

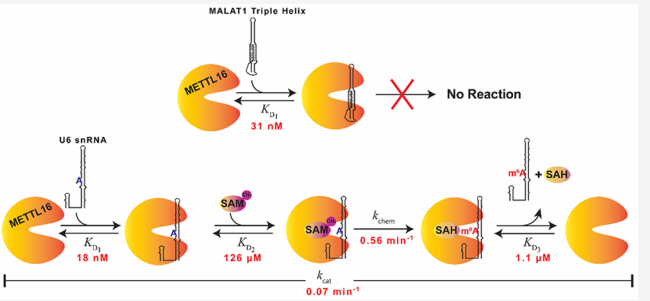

INTRODUCTION

Interest in RNA modifications has been revitalized due to advancements in detecting them,[1−3] in their expanding functional importance in RNA biology,[4,5] and in revealing new drug targets.[6,7] N^6-methyladenosine (m^{6}A) is a modification that is present in nearly all domains of life[8−11] and has been identified in various RNA classes, such as mRNA,[12,13] lncRNA,[12,14] rRNA,[15,16] snRNA,[17,18] and tRNA.[19] Notable physiological functions of m^{6}A sites in mRNA include stability,[20] splicing,[12] and translation initiation.[21] Despite m^{6}A being discovered in humans over 45 years ago, only recently have the methyltransferases responsible for "writing" m^{6}A marks been characterized.

Four human m^{6}A RNA methyltransferases have confirmed methylation activity, but only methyltransferase-like protein 3 (METTL3) of the METTL3/METTL14 complex (METTL14 is catalytically inactive but critical for RNA binding) and METTL16 catalyze the methylation of mRNAs.[15,18,22,23] The majority of m^{6}A marks in mRNAs and lncRNAs are introduced by METTL3/METTL14, a heterodimeric complex that methylates the underlined A in the DRACH (D = A, G, or U; R = A or G; H = A, C, or U) motif typically found near stop codons and 3′-UTRs of mRNAs.[3,23] In contrast, METTL16 has one established nonamer sequence motif, UACAGARAA, where the adenosine-to-be-methylated (underlined) is located within a bulge, hairpin, or single-stranded region flanked by double-stranded RNA.[18,24,25] Human METTL16 (Figure 1A) uses multiple regions to recognize RNA: the methyltransferase domain (1−291) consisting of an N-terminal region (1−78) and a highly conserved Rossmann fold (79−291) that has methyltransferase activity as well as the two vertebrate conserved regions (VCR) that share homology with terminal uridyltransferase (TUTase) and are required to bind some RNAs, such as U6 small nuclear RNA (snRNA, Figure 1B).[26] Despite the current knowledge about METTL16, there are many unknowns about METTL16-bound RNAs, their functions, and whether they are methylation targets of METTL16.

At present, METTL16 has several confirmed methylation targets: A43 in U6 snRNA (Figure 1B) and six hairpins (hp 1−6) in the 3′ UTR of the methionine adenosine transferase 2A transcript (MAT2A). All RNA substrates have the nonamer motif recognized by METTL16.[18] The evolutionarily conserved m^{6}A43 in U6 snRNA was recently shown in *Schizosaccharomyces pombe* to help stabilize base pairing

Received: October 20, 2022
Revised: December 2, 2022
Published: December 30, 2022

https://doi.org/10.1021/acs.biochem.2c00601
Biochemistry 2023, 62, 494−506

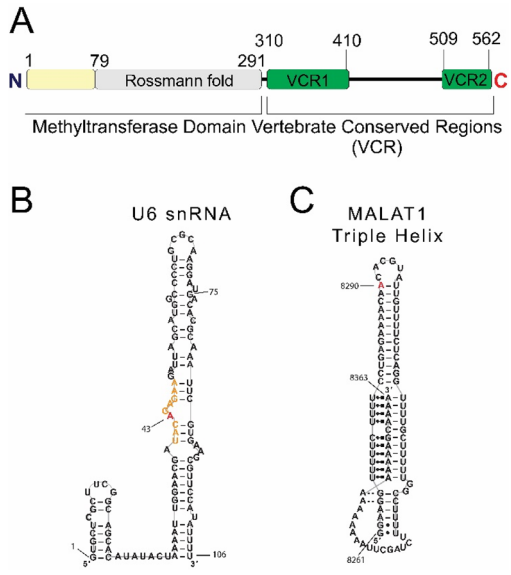

Figure 1. METTL16 and its RNA-binding partners. (A) Schematic showing the domain organization of METTL16: the N-terminal region (residues 1−78, yellow), the Rossmann fold (residues 79−291, gray), and the vertebrate conserved regions, VCR1 and VCR2 (residues 310−410 and 509−562, respectively, green). Schematics displaying the secondary structure of (B) U6 snRNA and (C) the MALAT1 RNA triple helix. The orange nucleotides denote the nonamer recognition motif of METTL16, and the red A is the adenosine associated with an m^{6}A signal (postulated for MALAT1).[1,17] Secondary structural interactions are represented as follows: Watson−Crick base pair (−), Hoogsteen base pair (●-■), A-minor interaction (--), and other noncanonical base pairs (●).

between U6 snRNA and the 5′ splice site of certain introns.[27] Although m^{6}A43 is evolutionarily conserved, it is uncertain if this function is conserved in higher eukaryotes because *Mettl16*-knockout mice embryos indicated no significant alterations in splicing.[24] METTL16 also methylates MAT2A hp 1−6. When SAM concentrations are low, hp1 is not methylated by METTL16, promoting the production of MAT2A, an enzyme that synthesizes nonhepatic SAM, the primary methyl donor in cells. Thus, METTL16 is considered a regulator of intracellular SAM concentrations.[18,28] Only a few substrates for methylation have been validated, although the RNA interactome of METTL16 includes numerous RNAs, such as the 3′-terminal triple helix of metastasis associated lung adenocarcinoma transcript 1 (MALAT1; Figure 1C).[29,30] Interestingly, a majority of the RNAs lack the UACAGARAA motif, so it is unclear if METTL16 catalyzes m^{6}A methylation at these sites.[29] Recently, m^{6}ACE-seq performed using RNA isolated from HEK293T cells located putative METTL16-dependent m^{6}A marks on RNAs with motifs similar to and different from the UACAGARAA motif, suggesting that there may still be unidentified RNA substrates of METTL16.[2]

Here, we sought to characterize the methylation pathways of METTL16 acting on the MALAT1 triple helix (Figure 1C), an RNA that lacks the nonamer motif, alongside a better-characterized RNA substrate, U6 snRNA (Figures 1B). Our results show that METTL16 employs a 1:1 binding stoichiometry with both the MALAT1 triple helix and U6 snRNA. METTL16 displays tight equilibrium dissociation constants (K_D) for the MALAT1 triple helix and U6 snRNA but methylates only U6 snRNA. For this RNA substrate, METTL16 utilizes an ordered bisubstrate mechanism, where the RNA is bound prior to the SAM methyl donor. Under single-turnover conditions, METTL16 exhibits a catalytic efficiency of 4.4×10^{-3} μM^{-1} min^{-1}, whereby the METTL16·RNA·SAM complex dissociates with a K_D of 126 μM, which would allow its activity to be regulated by the intracellular concentration of SAM. These insights into METTL16 will hopefully aid future studies regarding the function of m^{6}A43 in U6 snRNA, the role of METTL16 in regulating SAM, and therapeutic targeting of METTL16.

MATERIALS AND METHODS

Expression and Purification of METTL16. Two different expression plasmids were used in this study: pMCSG92 with an insert that encodes a C-terminally His$_6$-tagged human METTL16 (residues 1−562) and a pMCSG68 vector with an insert that encodes an N-terminally His$_6$-tagged human METTL16 methyltransferase domain referred to as METTL16_291 (residues 1−291; Table S1). Both plasmids were generated using the ligase-independent cloning method described previously,[31,32] and plasmid sequences were confirmed via Sanger sequencing (GENEWIZ). Each protein has a Ser−Asn−Ala linker to enable removal of His$_6$ tags via in-lab tobacco etch virus (TEV) protease. All METTL16 proteins were expressed in BL21 Gold *E. coli* (Agilent) and purified as previously described, excluding METTL16 prepared for native electrospray ionization mass spectrometry and microscale thermophoresis.[31] Human METTL16 used for native electrospray ionization mass spectrometry was purified as described previously except that size-exclusion chromatography utilized a mobile phase of 150 mM ammonium acetate (pH 5, adjusted using HCl), 150 mM KCl, 1 mM $MgCl_2$, and 5 mM tris(2-carboxyethyl)phosphine (TCEP); this step helped to generate a cleaner m/z spectrum. For microscale thermophoresis experiments, the TEV protease digest step was omitted so that the His$_6$ tag could bind to the RED-Tris-NTA fluorophore dye (METTL16-His$_6$).[31]

Preparation of RNA. The human MALAT1 triple helix and human U6 snRNA were prepared via *in vitro* transcription and splint RNA ligation (Table S2) while m^{6}A43 U6 snRNA was purchased from TriLink Biotechnologies. For *in vitro* transcribed RNA, sequences encoding the T7 promoter and the MALAT1 triple helix or U6 snRNA were inserted into a pHDV plasmid upstream of the HDV ribozyme as described previously.[33] Homemade T7 RNA polymerase was used to generate RNAs, which were subsequently gel purified as described previously.[34] Before each experiment, RNAs were folded in a buffer containing 10 mM HEPES (pH 7.5 at 20 °C), 150 mM KCl, and 10 mM $MgCl_2$; heated to 95 °C for 3 min; snap-cooled on ice for 5 min; and incubated 30 min at room temperature. U6 snRNA was prone to dimerizing at higher concentrations; therefore, it was folded at approximately 100 nM and then concentrated using an Amicon 10-kDa centrifugal filter (Millipore).

For site-specific [^{32}P]-radiolabeled RNA, a splint ligation technique adapted from previous methods was used.[18,35] RNA oligonucleotides for the MALAT1 triple helix and U6 snRNA (Table S2) were purchased from Sigma-Aldrich.[18] A single A (A8290 for MALAT1 and A43 for U6 snRNA) was 5′-end radiolabeled using γ-[^{32}P] ATP (~7000 Ci/mmol, PerkinElmer) and T4 PNK (NEB) per the manufacturer's protocol; reaction was heat inactivated at 95 °C for 5 min and then snap-cooled on ice for 3 min. To form the splint, the flanking RNA oligonucleotides and the corresponding DNA splint (Table

https://doi.org/10.1021/acs.biochem.2c00601
Biochemistry 2023, 62, 494−506

S2) were added to the T4 PNK mixture, heated to 85 °C for 2 min, and cooled to room temperature for 45 min. Then, DNA ligase (NEB, 2 000 000 units/mL) was added to ligate the RNA strands overnight at room temperature followed by 30 min of RQ1 DNase (Promega, 1 unit/μL) to digest the DNA splint. The splint-ligation reaction was loaded onto a 6% (w/v) denaturing polyacrylamide gel. Purified full-length RNA was excised and the gel piece crushed; 400 μL of G50 buffer (20 mM Tris-HCl (pH 7.5 at 20 °C), 300 mM sodium acetate and 2 mM EDTA) was added, freeze−thawed one time, and nutated at room temperature for 1 h before nutating overnight at 4 °C. The RNA-containing supernatant was then subjected to phenol-chloroform extraction and ethanol precipitation. The RNA pellet was reconstituted in 10 μL water and its concentration was determined using a Beckman LS6500 liquid scintillation counter. A body-labeled MALAT1 RNA triple helix was created by including α-[^{32}P] ATP (~6000 Ci/mmol, PerkinElmer) in the *in vitro* transcription reaction.

Microscale Thermophoresis. Microscale thermophoresis (MST) was employed to measure equilibrium dissociation constants ($K_{D1\ or\ 3}$) for the METTL16-His$_6$·RNA complexes. Full-length METTL16-His$_6$ was labeled using the Monolith His-Tag Labeling Kit RED-tris-NTA second generation according to the manufacturer's protocol. For the RNA-binding reaction, 20 nM labeled METTL16-His$_6$ was incubated with increasing amounts of prefolded MALAT1 triple helix, U6 snRNA, or m^{6}A43 U6 snRNA (~0.5 nM to 16.5 μM) in 10 mM HEPES (pH 7.5 at 20 °C), 150 mM KCl, 10 mM $MgCl_2$, 1 mM dithiothreitol (DTT), and 0.01% Tween-20. Samples were allowed to equilibrate for at least 30 min at room temperature prior to scanning at the default settings. After scanning, MO.Affinity.Analysis software (version 2.3) generated plots of intensity versus RNA concentration and applied the following equation:

$$f(c) = \text{Unbound} + (\text{Bound} - \text{Unbound}) \times \frac{c + c_{target} + K_{D1or3} - \sqrt{(c + c_{target} + K_{D1or3})^2 - 4 \times c \times c_{target}}}{2c_{target}} \quad (1)$$

where $f(c)$ is the fraction bound at a given ligand concentration c, the Unbound is the F_{norm} signal of the target alone, Bound is the F_{norm} signal of the complex, $K_{D1\ or\ 3}$ is the equilibrium dissociation constant of METTL16-His$_6$·RNA, and c_{target} is the final concentration of the target in the assay. Using a previously established method,[36] saturation binding curves were performed under the same conditions except that the METTL16 concentrations used were 600 nM and 400 nM for the MALAT1 triple helix and U6 snRNA, respectively. A narrow titration of each RNA was used near the respective concentration of METTL16. The saturated and unsaturated data points were linearly fit, and the x intercepts of linear fits extrapolated the RNA concentration, which was compared to the METTL16 concentration in the binding reactions to determine RNA/protein binding stoichiometry.

Native Electrospray Ionization Mass Spectrometry. METTL16 was buffer exchanged into 150 mM ammonium acetate (pH 7.5) using an Amicon Ultra-15 Centrifugal Filter Unit 30-kDa cutoff (Millipore). The MALAT1 triple helix was folded by heating at 95 °C for 3 min and snap-cooling on ice for 5 min in a buffer of 150 mM ammonium acetate (pH 7.5) and 10 mM $MgCl_2$, whereas U6 snRNA was folded in 150 mM ammonium acetate (pH 7.5). Both RNA samples were buffer exchanged with 500 volumes of 150 mM ammonium acetate to remove any residual salts. METTL16·RNA complexes were formed by combining the components after buffer exchange. All samples (METTL16 and METTL16·RNA complexes) were analyzed at 5 μM (i.e., 5 μM RNA and 5 μM METTL16 were pre-equilibrated to form the complex). Instrument parameters of an Impact II (Bruker, Billerica, MA) quadrupole time-of-flight mass spectrometer fitted with an electrospray ionization source included positive-ion mode, an end plate offset of 0.4 kV, a capillary voltage of 1.8 kV, a nebulizer gas pressure of 4.0 bar, a dry gas flow rate of 7.0 L/min, a dry gas temperature of 200 °C, a funnel 1 RF of 400 V, a funnel 2 RF of 600 V, a hexapole RF of 700 V, a quadrupole ion energy of 3.0 eV, a collision energy of 10 eV, a collision cell RF of 4.2 kV, an ion transfer time of 120 μs, and a prepulse ion storage of 30 μs. The samples were infused at a flow rate of 3 μL/min, and data were acquired over the m/z range of 1000−10 000 unified atomic mass units (u).

Liquid Chromatography Electrospray Ionization Tandem Mass Spectrometry (LC/ESI-MS/MS). A mass spectrometry approach adapted from earlier studies was utilized to verify the presence or absence of m^{6}A in the MALAT1 triple helix and U6 snRNA.[37] *In vitro* methyltransferase reactions (500 μL) were set up with METTL16 (16 μM), either MALAT1 triple helix RNA or U6 snRNA (4 μM), and SAM (1 mM; Cayman Chemical Item No. 13956) in the optimized buffer (refer to pre-steady-state kinetic assays) at 37 °C for 30 min. After isolating the RNA using phenol-chloroform extraction and ethanol precipitation, 1 μg of RNA was digested with two units of Nuclease P1 (Sigma) in 10 μL of 30 mM sodium acetate (pH 5.2) at 37 °C for 5 h. The reaction volume was increased to 100 μL by adding 5 μL of 0.002 U/μL phosphodiesterase I (Sigma), 1.5 μL of 20 U/μL CIAP (Promega), and 1× CIAP buffer. The mix was given an additional 2 h to completely digest RNA into nucleosides. Another 100 μL of water was added once digestion was completed, and the solution was chloroform extracted twice. The aqueous solution was then lyophilized to dryness using a FreeZone 2.5 Liter −84 °C Benchtop Freeze-Dryer and reconstituted in 100 μL of RNase-free water.

A Bruker micrOTOF-II instrument using an Acquity UPLC HSS T3 column with 1.8 μm particle size and 2.1 × 150 mm dimensions was used to resolve nucleosides. Nucleoside standards (C, U, A, G) were purchased from Sigma, and an N^6-methyladenosine standard was purchased from Abcam. The digested MALAT1 triple helix, U6 snRNA, and standards were run with solvent A (water with 0.1% formic acid) and solvent B (acetonitrile with 0.1% formic acid). A flow rate of 0.4 mL/min was kept constant during the following gradient elution: 0 min, 0% B; 2 min, 0% B; 14 min, 20% B; 16 min, 50% B; 16.1 min, 0% B; and 20 min, 0% B. The standard nucleosides and N^6-methyladenosine were detected using extracted ion chromatograms (EIC) set for the ions of 244.1 (C), 245.1 (U), 268.1 (A), 284.1 (G), and 282.1 (m^{6}A).

Presteady-State Kinetic Assays. The buffer optimization assays contained 250 nM METTL16 preincubated with 1 μM U6 snRNA and 200 μM SAM to start the reactions. The following components were held constant except for the component being varied: 10 mM HEPES (pH 7.5 at 20 °C), 150 mM KCl, 10 mM $MgCl_2$, and 1 mM TCEP. Optimal buffer conditions were determined to be 10 mM HEPES (pH 7.5 at 20 °C), 150 mM KCl, 10 mM $MgCl_2$, and 5 mM TCEP at 37 °C.

https://doi.org/10.1021/acs.biochem.2c00601
Biochemistry 2023, 62, 494−506

Scheme 1

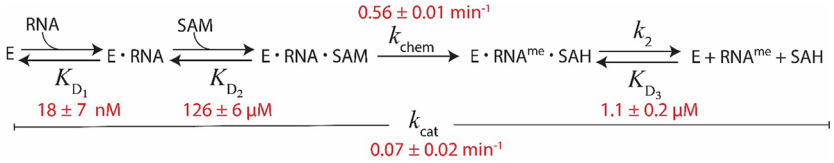

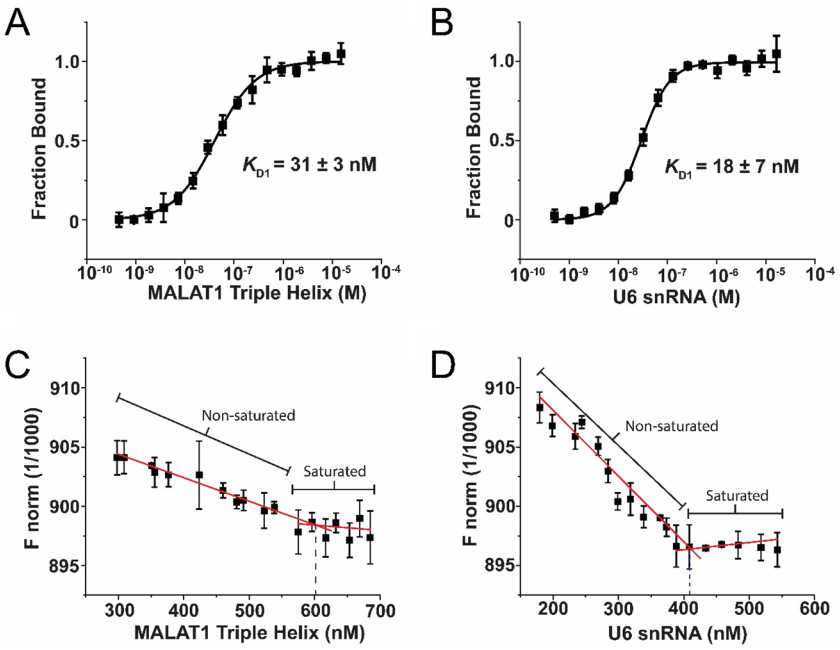

Figure 2. Binding affinities and stoichiometries of the METTL16·MALAT1 triple helix and METTL16·U6 snRNA. MST analysis of binding interactions between METTL16 and (A) the MALAT1 triple helix, measuring a K_{D1} of 31 ± 3 nM, and (B) U6 snRNA, measuring a K_{D1} of 18 ± 7 nM. The K_{D1} values were obtained from fitting data points representing averages of three independent runs, and the reported error is from data fitting. Error bars represent the standard deviation of three independent runs. Saturation curves performed in triplicate indicate 1:1 binding stoichiometry for the (C) METTL16·MALAT1 triple helix and (D) METTL16·U6 snRNA complexes. Error bars represent standard deviation from three independent trials.

The equilibrium dissociation constant for the METTL16·U6 snRNA·SAM complex was determined in the optimal reaction buffer under the following single-turnover reaction conditions: 5 μM METTL16 pre-equilibrated with 0.5 μM U6 snRNA and time courses initiated with 10, 50, 100, 250, 500, and 1000 μM SAM. The assays using METTL16_291 were set up similarly (i.e. 5 μM enzyme preincubated with 0.5 μM U6 snRNA), except time courses were initiated with 10, 50, 100, 250, 500, 1000, 1250, 1500, and 1750 μM SAM.

Preincubation Assays. Three reactions were prepared whereby METTL16 (200 nM) was preincubated for 1 h on ice with SAM (1 mM), RNA (2 μM), or neither substrate, and the reactions were initiated by adding 2 μM RNA, 1 mM SAM, or both 2 μM RNA and 1 mM SAM, respectively.

Isotope Partitioning Assays. METTL16 (1 μM) was preincubated with radiolabeled U6 snRNA (1 μM) in two aliquots of 10 μL, and the two parallel reactions were increased to 120 μL with either 1 μM radiolabeled U6 snRNA in one reaction (i.e., "hot" chase) or unlabeled U6 snRNA (i.e., "cold" chase) along with 1 mM SAM to initiate the reaction.

Steady-State Kinetic Assays. Methylation reactions were completed under steady-state conditions: 200 nM METTL16 preincubated with 2 μM U6 snRNA. Various SAM concentrations were added to start the reaction: 50, 100, 250, 500, and 1000 μM.

Product Analysis for *in Vitro* Methyltransferase Assays. Methylation reactions were quenched by transferring 10 μL aliquots of the reaction mixture to 100 μL of phenol-chloroform at various times. RNA underwent ethanol precipitation, and the pellet was resuspended in 3 μL of 0.33 U/μL Nuclease P1 (Sigma-Aldrich) in 30 mM sodium acetate at pH 5.2 and 6.7% glycerol. After digesting RNA for 2 h at 37 °C, 1 μL of digested RNA was spotted onto a cellulose TLC plate (MP Biomedicals). Adenosine and m^{6}A were separated using a solvent composed of isopropanol/hydrochloric acid/water (70:15:15 by volume) for 14−20 h.[18] Plates were air-dried for 1 h, wrapped in plastic wrap, exposed to a Phoshorimager screen overnight, and scanned using an Amersham Typhoon Phosphorimager (GE Healthcare). ImageQuant TL (ver. 8.1) was used for quantitation of [^{32}P]-A and [^{32}P]-m^{6}A signals.

Data Analysis for *in Vitro* Methyltransferase Assays. Data were fit using Origin 2018b for linear and nonlinear regression analyses.

For the pre-steady state, the resulting m^{6}A product concentration was plotted against time and fitted to eq 2:

$$y = A \times (1 - e^{(-k_{obs} \times t)}) \quad (2)$$

where A is the scaling constant, k_{obs} is the observed rate constant, and t is the time in minutes.[38] The pre-steady state

https://doi.org/10.1021/acs.biochem.2c00601
Biochemistry 2023, 62, 494−506

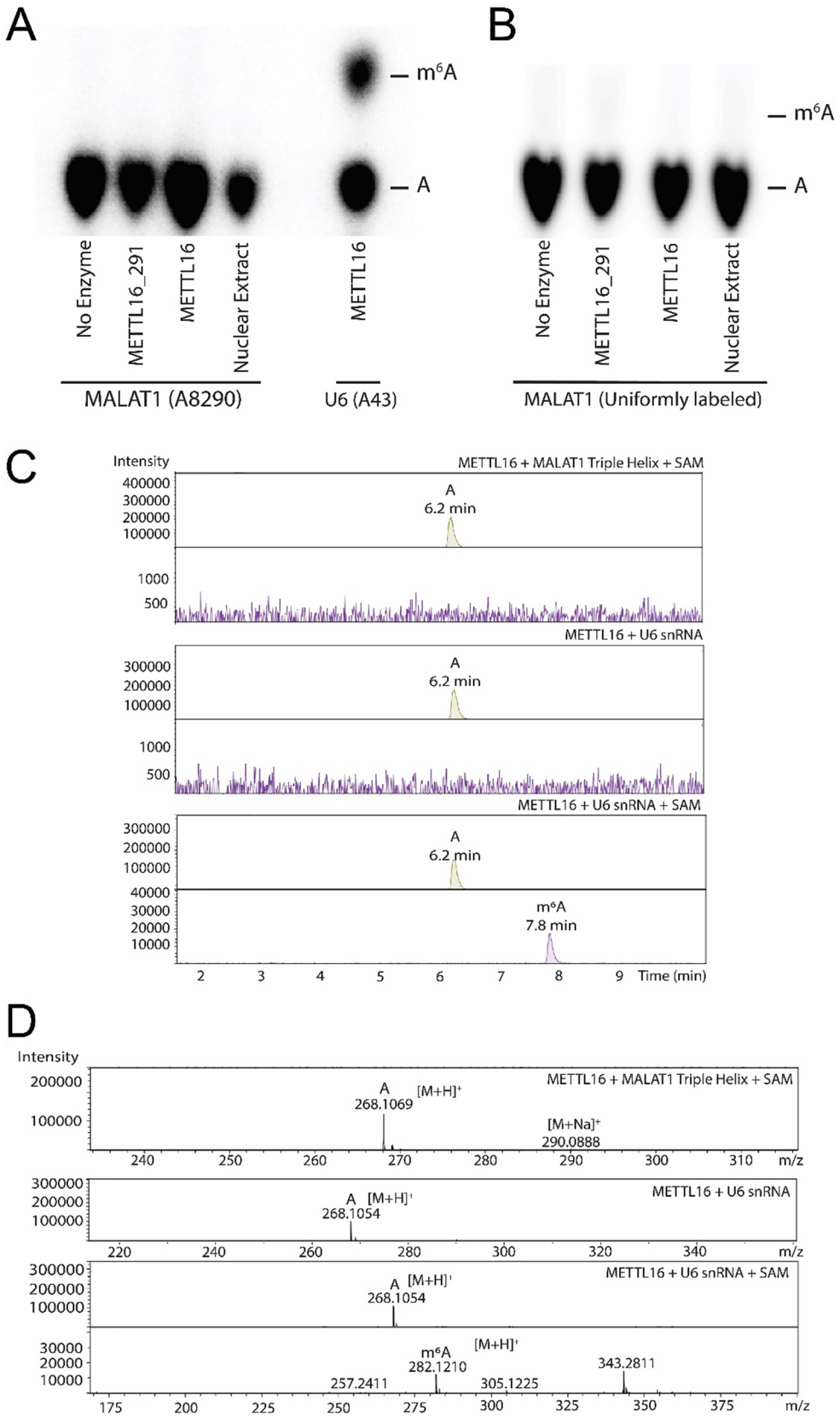

Figure 3. The MALAT1 triple helix is not methylated by METTL16 *in vitro*. No m^6A signals were detected when (A) [^{32}P]-labeled A8290 MALAT1 triple helix or (B) α-[^{32}P]-AMP-body-labeled MALAT1 triple helix was incubated with the methyltransferase domain of METTL16 (METTL16_291), full-length METTL16, or nuclear extract. (C) Chromatograms and (D) mass spectra of the following RNase-digested reactions: METTL16+MALAT1 triple helix+SAM, METTL16+U6 snRNA, and METTL16+U6 snRNA+SAM. Nucleoside identity was determined using chromatograms and mass spectra of purchased standards: C, U, A, G, and m^6A (Figure S3).

https://doi.org/10.1021/acs.biochem.2c00601
Biochemistry 2023, 62, 494−506

rate constants (k_{obs}) were then plotted against the corresponding SAM concentrations (μM) and fitted to a hyperbolic equation:

$$k_{obs} = \frac{k_{chem} \times C}{K_{D2} + C} \quad (3)$$

where k_{obs} is the observed rate constant, k_{chem} is the single-turnover rate constant (i.e., rate encompassing steps from METTL16 preincubated with RNA to methyl transfer), C is the concentration of SAM, and K_{D2} is the apparent dissociation constant.[38]

For preincubation, isotope partitioning, and steady-state kinetic assays, plots of m^{6}A product versus time were linearly fit to eq 4:

$$y = v_o \times t \quad (4)$$

where y is the measured m^{6}A product (or pixel signal intensity for isotope partitioning assays), v_o is the initial velocity, and t is the time. Time points incorporating zero minutes for the data result in the plots having a y intercept of zero. For steady-state analyses, the initial velocities were plotted against the concentration of substrate and fitted to the Michaelis−Menten equation:

$$v_o = \frac{V_{max} \times [S]}{K_M + [S]} \quad (5)$$

where v_o is the initial velocity, V_{max} is the maximal velocity, K_M is the substrate concentration at half V_{max}, and [S] is the substrate concentration. The catalytic rate constant (k_{cat}) was obtained by dividing V_{max} by the total enzyme concentration ($[E]_T$).

Isoelectric Focusing Gel. A pH 3−10 Criterion isoelectric focusing (IEF) gel (Bio-Rad) was run per the manufacturer's protocol using full-length METTL16 as well as IEF standards from Bio-Rad (Cat. 1610310). The gel was then fixed using a 4% sulfosalicylic acid, 12.5% trichloroacetic acid, and 30% methanol solution for 30 min on a shaker. After removing the fixing solution, a destaining solution of 12% ethanol, 7% acetic acid, and 0.5% $CuSO_4$ was used to remove the background, and then a solution of 25% ethanol and 7% acetic acid was used to remove trace $CuSO_4$. The gel was imaged using an Azure c400.

RESULTS

METTL16 Binds to the MALAT1 Triple Helix and U6 snRNA with Similar Affinity and a Binding Stoichiometry of 1:1. To better understand the interaction between METTL16 and the MALAT1 triple helix, we employed microscale thermophoresis (MST) to measure the K_{D1} (Scheme 1). A relatively tight K_{D1} value of 31 ± 3 nM was determined for the METTL16-His$_6$·MALAT1 triple helix complex (Figure 2A, Table 1). Because U6 snRNA has the nonamer motif and is a major cellular target of METTL16,[18] we repeated the MST experiments using U6 snRNA and obtained a K_{D1} value of 18 ± 7 nM for the METTL16-His$_6$·U6 snRNA complex (Figure 2B, Table 1). These results suggested that METTL16 forms a relatively tight binary complex with the MALAT1 triple helix and U6 snRNA.

Previous studies have shown that apo METTL16 is a monomer.[24,25] However, previously published native gel-shift assays of METTL16·MAT2A hp and METTL16·U6 snRNA complexes revealed multiple RNP bands.[25,26] Therefore, using MST, saturation binding curves were generated to determine the binding stoichiometry of METTL16 with the MALAT1 triple helix and U6 snRNA.[36] Fluorophore-tagged METTL16 was prepared at concentrations 20-times the established K_D values for the MALAT1 triple helix and U6 snRNA with a narrow titration of the respective RNAs near the concentration of METTL16. As more RNA is added, the MST signal from fluorophore-tagged METTL16 decreases until saturation occurs, i.e., the signal no longer changes with the addition of more RNA. Linear fits of the unsaturated and saturated points intersect at the breakpoint, which reveals the METTL16/RNA ratio. For the MALAT1 triple helix, 600 nM METTL16 reached saturation at 601.7 nM of the RNA, resulting in a binding stoichiometry of 1:1 for the METT16/MALAT1 triple helix complex (Figure 2C). Saturation of 400 nM METTL16 with U6 snRNA occurred at 410.8 nM, indicating that one METTL16 protein binds to one U6 snRNA (Figure 2D). Native electrospray ionization mass spectrometry (ESI-MS) was utilized to determine that apo METTL16 is a monomer (Figure S1A). A 1:1 binding stoichiometry for the METTL16·MALAT1 triple helix and METTL16·U6 snRNA complexes was also observed using native ESI-MS (Figure S1B,C). Our *in vitro* binding assays suggest that METTL16 interacts relatively tightly with the MALAT1 triple helix, which lacks the nonamer motif, and U6 snRNA at a 1:1 ratio; therefore, the multiple bands of METTL16·RNA in gel-shift assays may reflect different conformational states.

MALAT1 Triple Helix Is Not a Substrate of METTL16 *in Vitro*. Our next objective was to determine if the MALAT1 triple helix has any METTL16-dependent m^{6}A sites. The m^{6}A individual-nucleotide resolution cross-linking and immunoprecipitation (miCLIP) method, in particular the cross-linking induced mutation sites (CIMS) analysis, detected one m^{6}A mark, albeit weakly, near A8290 in the MALAT1 triple helix (Figure 1C) isolated from HEK293 cells.[1] Therefore, we used an *in vitro* methyltransferase assay to determine if METTL16 could catalyze methylation at A8290 under optimal reaction buffer conditions. No m^{6}A signal was detected when the [^{32}P]-A8290-MALAT1 triple helix was in the presence of METTL16_291, METTL16, or nuclear extract (Figure 3A), although an m^{6}A43 signal was detected for U6 snRNA (Figure S2).

It is possible that an adenosine other than A8290 is methylated by METTL16. Therefore, we repeated the assay using a uniformly α-[^{32}P]AMP-labeled MALAT1 triple helix, but again there was no m^{6}A signal (Figure 3B). With 30 adenosines being labeled, it is possible that the m^{6}A signal is below the detection limit. Therefore, we employed an orthologonal method: LC/ESI-MS/MS.[37] Using LC/ESI-MS/MS, we ran nucleoside standards of C, U, A, G, and m^{6}A to ascertain retention times and to confirm the mass to charge (m/z) ratio to expected values (Figure S3). A discernible mass spectrum signal that corresponded to the m^{6}A nucleoside was detected for the U6 snRNA incubated with METTL16 and SAM but not the analogous reaction containing the MALAT1 triple helix (Figure 3C,D). Under the conditions tested herein, these results suggest that the MALAT1 triple helix is not methylated by METTL16 *in vitro*. Henceforth, our kinetic investigation of METTL16 focused on only U6 snRNA.

Optimization of Reaction Buffer for Methyltransferase Activity of METTL16. In our initial kinetic experiments, METTL16 exhibited minimal catalytic activity for the U6

https://doi.org/10.1021/acs.biochem.2c00601
Biochemistry 2023, 62, 494−506

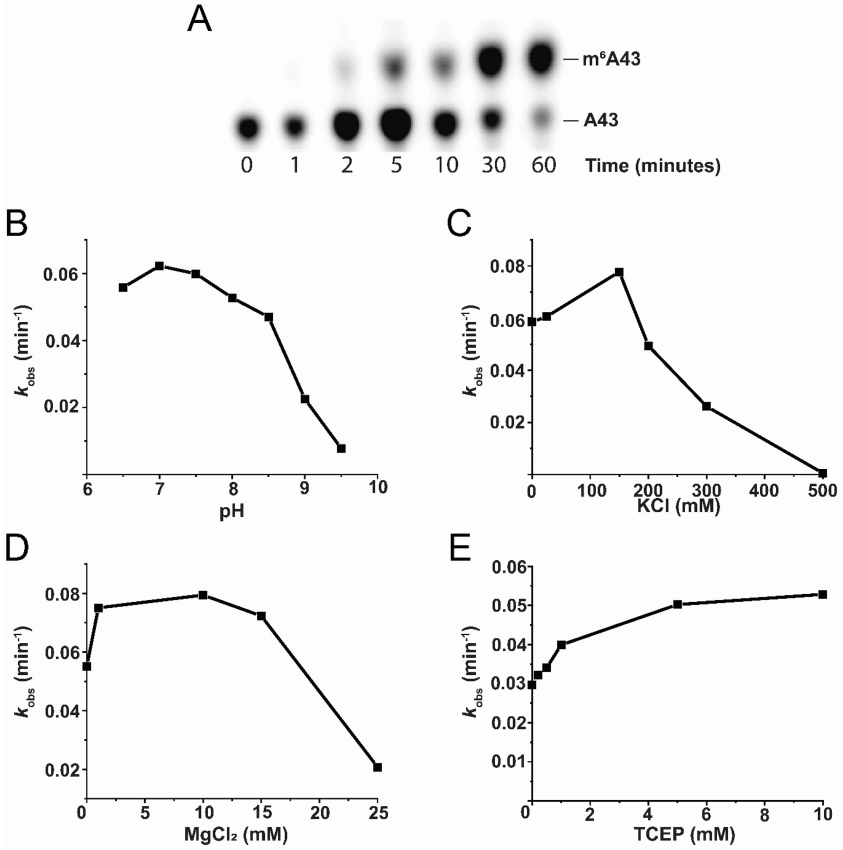

Figure 4. Methyltransferase activity of METTL16 depends on buffer conditions. (A) TLC was used to separate the [^{32}P]-labeled A43 mononucleoside from the [^{32}P]-labeled m^{6}A43 product. A representative image is shown for a time course with an observed methylation rate of 0.05 min^{-1} at 37 °C. Methyltransferase activity of METTL16 was measured, and plots are shown for the k_{obs} values as a function of (B) pH, (C) KCl, (D) $MgCl_2$, and (E) TCEP. All assays contained 250 nM METTL16 preincubated with 1 μM U6 snRNA and were initiated with 200 μM SAM with the following components held constant at 10 mM HEPES (pH 7.5 at 20 °C), 150 mM KCl, 10 mM $MgCl_2$, and 1 mM TCEP except for the component being varied.

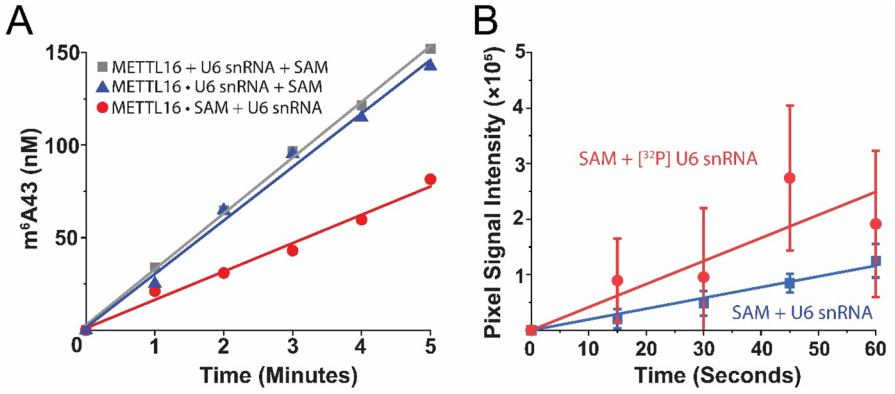

Figure 5. METTL16 binds U6 snRNA prior to SAM. (A) Preincubation assays of METTL16 initiated with both substrates (gray ■), METTL16 preincubated with SAM and initiated with U6 snRNA (red ●), and METTL16 preincubated with U6 snRNA and initiated with SAM (blue ▲). Rates are an average of five independent trials, and the error represents standard deviation. A representative replicate is shown. (B) Isotope partitioning assay with METTL16•[^{32}P]-A43 U6 snRNA chased with either unlabeled U6 snRNA (blue ■) or [^{32}P]-A43 U6 snRNA (red ●) in the presence of SAM suggested that the METTL16·U6 snRNA complex is competent. Error bars represent standard deviation of values from three independent runs.

snRNA substrate, emphasizing the need to optimize the reaction buffer. To examine how the methyltransferase activity of METTL16 depends on reaction conditions, all reaction components were held constant while the buffer pH, ionic strength (KCl, $MgCl_2$, $ZnCl_2$), reducing agent (TCEP), or bovine serum albumin (BSA) were varied systematically in an *in vitro* methyltransferase assay. The rate of methylation was not greatly affected by TCEP or BSA, was inhibited by $ZnCl_2$, and had observable optima for buffer pH, KCl, and $MgCl_2$ (Figure 4, Figure S4).

Based on k_{obs} values, the maximal rate of methylation was observed at pH 7, 150 mM KCl, 10 mM $MgCl_2$, and 10 mM

https://doi.org/10.1021/acs.biochem.2c00601
Biochemistry 2023, 62, 494−506

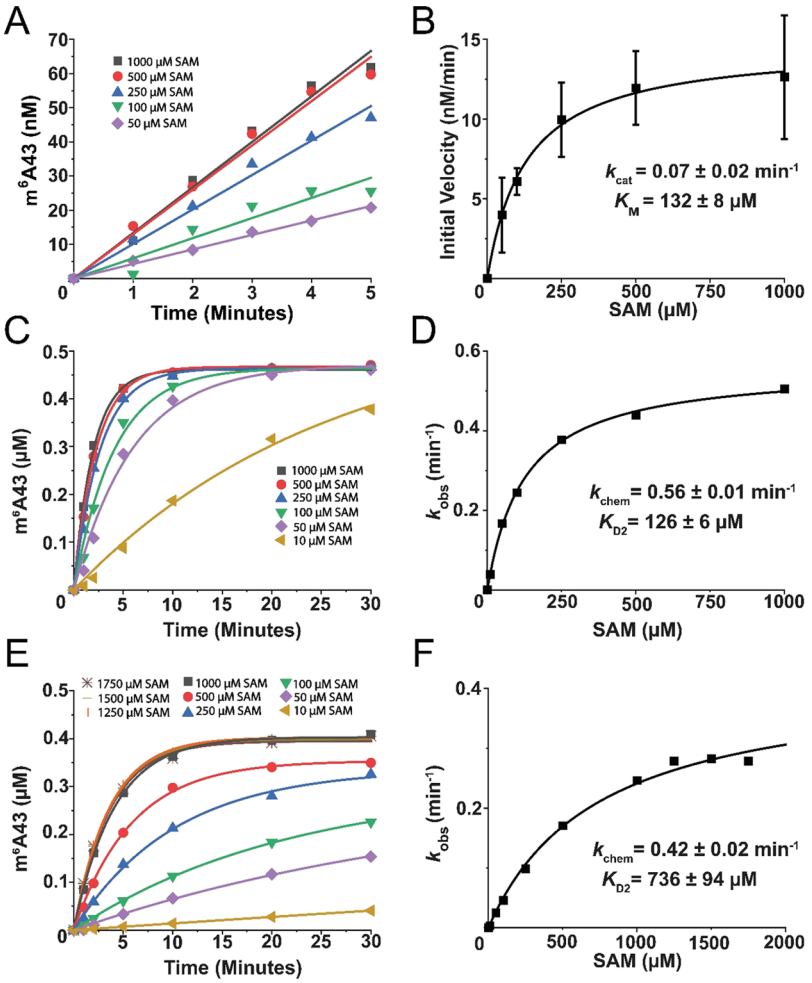

Figure 6. Steady-state assays and pre-steady-state assays with METTL16. All reactions contained 20 mM HEPES (pH 7.5 at 20 °C), 150 mM KCl, 10 mM $MgCl_2$, and 5 mM TCEP. (A) Steady-state kinetic assays contained 200 nM METTL16 and 2 μM U6 snRNA added to various concentrations of SAM (50−1000 μM). Data points are averages of three independent trials. (B) Extrapolated steady-state kinetic parameters from the plot were a k_{cat} of 0.07 ± 0.02 min^{-1} and K_M of 132 ± 8 μM. The values are an average of three independent trials, and the error represents standard deviation. (C) Pre-steady-state kinetic assays contained 5 μM METTL16 preincubated with 0.5 μM U6 snRNA added to various concentrations of SAM (1−1000 μM). (D) A k_{chem} of 0.56 ± 0.01 min^{-1} and K_{D2} of 126 ± 6 μM were extrapolated. (E) Pre-steady-state kinetic assays contained 5 μM METTL16_291 preincubated with 0.5 μM U6 snRNA mixed with various concentrations of SAM (50−1750 μM). (F) Extrapolated pre-steady-state kinetic parameters from the plot were a k_{chem} of 0.42 ± 0.04 min^{-1} and K_{D2} of 736 ± 94 μM. All reported error values for pre-steady-state kinetic assays are from data fitting.

TCEP (Figure 4). The highest rate of methylation occurred at pH 7, which is approximately one pH unit from the theoretical pI of 8.08 calculated by ExPASy[39] and our value of approximately 8 determined from an isoelectric focusing gel (Figure S5). However, the percent difference between the k_{obs} of pH 7 and 7.5 is less than 3% (Figure 4B); therefore, a pH of 7.5 was used to remain near physiological pH and to satisfy MST conditions, which require pH > 7 for fluorophore labeling. Last, 5 mM TCEP was chosen because the activity increase between 5 and 10 mM TCEP was minimal: from 0.050 min^{-1} to 0.053 min^{-1} (Figure 4E). An optimal buffer for METTL16 catalyzing the methylation of U6 snRNA was determined to be 10 mM HEPES (pH 7.5 at 37 °C), 150 mM KCl, 10 mM $MgCl_2$, and 5 mM TCEP.

METTL16 Binds to U6 snRNA First Followed by SAM. As a methyltransferase, METTL16 may, in theory, first form a binary complex with either RNA or SAM. Unfortunately, we were unable to measure the binding affinity of the METTL16·SAM binary complex using filter-binding assays, isothermal titration calorimetry, and MST (data not shown). In the literature, METTL16 reportedly employs a random-order binding mechanism with the MAT2A hp1 and SAM based on a preincubation assay,[40] whereas crystallographic studies of METTL16 (residues 1−310) bound to a truncated MAT2A hp suggested that SAM could not enter the active site if the RNA was already bound.[25] To determine if methylation of U6 snRNA depends on substrate-binding order, two different assays were performed: preincubation and isotope partitioning assays. Under steady-state conditions, METTL16 was preincubated for an hour with either U6 snRNA (METTL16·U6 snRNA + SAM), SAM (METTL16·SAM + U6 snRNA), or neither (METTL16 + U6 snRNA + SAM), and then the reaction was initiated by adding the missing substrate(s). The rate of methyl transfer was about 2-fold slower when METTL16 was preincubated with SAM (13 ± 4 nM/min) versus U6 snRNA (27 ± 9 nM/min). No substrate preloading resulted in a rate (24 ± 7 nM/min) similar to the METTL16·U6 snRNA preincubation complex (Figure 5A).

These results suggest that U6 snRNA binds prior to SAM. To provide further support for this binding order, an isotope

https://doi.org/10.1021/acs.biochem.2c00601
Biochemistry 2023, 62, 494−506

Table 1. Summary of Kinetic Parameters

METTL	METTL16	METTL16	METTL16	METTL3/14
RNA substrate	MALAT1 triple helix	U6 snRNA	MAT2A hairpin 1	DRACH motif-containing RNA
K_{D1} (E·RNA)	31 ± 3 nM	18 ± 7 nM (16 ± 2 nM, Aoyama)	42 ± 6 nM (Aoyama)	~10 μM (Wang)
K_{D2} (E·SAM)	N/A	126 ± 6 μM[a]	TBD	1.5 ± 0.2 μM (Wang)
K_{D3} (E·RNA^{me})	N/A	1.1 ± 0.2 μM	TBD	TBD
K_M (SAM)	N/A	132 ± 8 μM	>0.4 mM (Yu)	102 ± 15 nM (Li)
k_{cat} (SAM)	N/A	0.07 ± 0.02 min^{-1}	TBD	0.3 ± 0.03 min^{-1} (Li)
k_{chem}	no observable activity	0.56 ± 0.01 min^{-1}	TBD	TBD
k_{cat}/K_M (SAM)	N/A	5.3 × 10^{-4} μM^{-1}min^{-1}	TBD	2.9 μM^{-1}min^{-1} (Li)
k_{chem}/K_{D2} (SAM)	N/A	4.4 × 10^{-3} μM^{-1}min^{-1}	TBD	TBD
reference	this study	this study; Aoyama et al.[26]	Aoyama et al.;[26] Yu et al.[40]	Wang et al.;[42] Li et al.[43]

[a]Denotes that the value is representative of the METTL16·U6 snRNA·SAM complex. "N/A" denotes that the kinetic parameter cannot be measured. "TBD" denotes that the kinetic parameter has not yet been reported.

partitioning assay was performed. METTL16 (1 μM) was preincubated with radiolabeled U6 snRNA (1 μM) in two aliquots, and then a 12-fold molar excess of either radiolabeled or unlabeled U6 snRNA was added at the same time as 1 mM SAM to initiate the reaction. If SAM must bind first, then the radiolabeled METTL16·U6 snRNA complex would need to dissociate, and little radioactive product formation would be detected because METTL16 would be prone to methylating unlabeled U6 snRNA. We observed similar rates of methylation for both reactions: (0.042 ± 0.027) × 10^5 pixels/s for the radiolabeled RNA chase and (0.019 ± 0.005) × 10^5 pixels/s for the unlabeled RNA chase (Figure 5B). The rates seem to suggest that the METTL16·U6 snRNA complex was competent, i.e., able to bind SAM and proceed to the methyl transfer step. In other words, METTL16 does not require U6 snRNA to dissociate to allow SAM to bind first. We conclude that the methylation of U6 snRNA proceeds through an ordered-sequential pathway, whereby METTL16 binds to the U6 snRNA followed by SAM (Scheme 1).

Rate-Limiting Step of the METTL16-U6 snRNA Kinetic Pathway Is Likely Product Release. For additional mechanistic insights, we performed kinetic assays under steady-state and pre-steady-state reaction conditions. The assay performed under steady-state conditions (*i.e.* METTL16 (0.2 μM)·U6 snRNA (2 μM)) mixed with increasing concentrations of SAM yielded the following kinetic parameters: a K_M of 132 ± 8 μM and a k_{cat} of 0.07 ± 0.02 min^{-1} (Figure 6A,B, Table 1).

K_M reflects the concentration of SAM needed to obtain half-maximal activity, and k_{cat} reflects the rate of multiple turnovers, i.e., the step from apo METTL16 and RNA (E + RNA) to free enzyme and products (E + RNA^{me} + SAH; Scheme 1). For other methyltransferases, it has been shown that pre-steady-state kinetic assays can provide the rate of the methylation step, the K_D values for substrates, and whether the pre-steady-state rate relative to the steady-state reveals any rate limitations.[38,41] Based on what we know about the METTL16·U6 snRNA reaction pathway thus far, pre-steady-state kinetic assays can determine the equilibrium dissociation constant (K_{D2}) of the METTL16·U6 snRNA·SAM ternary complex and a rate constant that would encompass the steps from the METTL16·U6 snRNA binary complex through methyl transfer (k_{chem}; Scheme 1). Various concentrations of SAM were mixed with the METTL16 (5 μM)·U6 snRNA (0.5 μM) binary complex to initiate the reaction. Plots of k_{obs} values versus SAM concentrations (Figure 6C,D) were fit to a hyperbolic equation (eq 3). The resulting K_{D2} was 126 ± 6 μM and k_{chem} was 0.56 ± 0.01 min^{-1}. These results suggest that METTL16 binds to RNA with much greater affinity than SAM, providing additional support for the ordered-sequential mechanism. Similar K_{D2} and K_M values indicate that the k_{cat} is much slower than the rate of substrate dissociation from the enzyme (*i.e.* k_{off} for the METTL16·U6 snRNA complex). The 8-fold difference between k_{chem} and k_{cat} suggests that steps following methylation are limiting k_{cat}. Thus, product dissociation is likely the rate-limiting step in the METTL16 kinetic pathway. METTL16 binds weakly to m^{6}A43 U6 snRNA; a K_{D3} of 1.1 ± 0.2 μM was measured using MST (Figure S6, Table 1). This result indicates that METTL16 exhibits an approximately 60-fold weaker binding affinity for the methylated U6 snRNA than the substrate, suggesting a strong selectivity for binding unmethylated U6 snRNA.

Next, we wanted to probe the rate-limiting step of k_{chem}, which is generally thought to be either a conformational change or the chemistry of methyl transfer. Earlier work proposed that binding of the C-terminal VCR regions to U6 snRNA would induce a conformational rearrangement of the methylation site to render a catalytically competent complex.[26] Such a conformational rearrangement could potentially limit k_{chem}. Therefore, we measured k_{chem} and K_{D2} for the methyltransferase domain of METTL16 (i.e., METTL16_291), which lacks the two VCRs, methylating U6 snRNA under pre-steady-state conditions (Figure 6E,F). A k_{chem} of 0.42 ± 0.02 min^{-1} is similar to k_{chem} measured for full-length METTL16, suggesting that the structural changes of U6 snRNA induced by the C-terminal VCR regions do not limit the rate of methylation. However, the VCR domains do enhance formation of the ternary complex, for the K_{D2} of METTL16_291·U6 snRNA·SAM is 736 ± 94 μM, which is approximately 6-fold weaker than full-length METTL16·U6 snRNA·SAM (Figure 6D,F). Overall, these results show that the C-terminal VCRs of METTL16 promote formation of the ternary complex but have a minimal 1.3-fold decrease on the k_{chem} rate constant for METTL16_291, suggesting the VCRs are not involved in limiting k_{chem}.

DISCUSSION

METTL16 interacts with a myriad of RNAs, using a combination of sequence and structure to recognize them.[24,29] Some RNAs are methylated by METTL16, while others are not. In this study, our MST results show that METTL16 can bind relatively tightly to the MALAT1 triple

https://doi.org/10.1021/acs.biochem.2c00601
Biochemistry 2023, 62, 494−506

helix at 31 nM and U6 snRNA at 18 nM (Figure 2A,B, Table 1), but the MALAT1 triple helix is not methylated by METTL16 under *in vitro* reaction conditions (Figure 3). The MALAT1 triple helix lacks the UACAGAGAA nonamer motif that the U6 snRNA and MAT2A hairpins possess for methylation (Figure 1C); however, A8290 resides in a CAACA sequence that more closely resembles the DRACH motif recognized by the METTL3/METTL14 complex.[3,44−48] It is possible that the METTL3/METTL14 complex is responsible for the weak m^{6}A signal detected using cross-linking-induced mutation sites (CIMS) from miCLIP data, although we did not detect any methylation signal in the presence of nuclear extract (Figure 3A) despite observing methylation activity on U6 snRNA with nuclear extract (Figure S2).[1] Another possibility is that additional protein cofactors are required and/or A8290 is methylated in the MALAT1 precursor, which has the tRNA-like structure of MALAT1-associated small cytoplasmic RNA (mascRNA) downstream of the region known to form a triple helix.[49] However, it is important to note that all confirmed RNA substrates of METTL16 have the targeted adenosine unpaired, likely for the base to freely flip into the active site. If an unpaired adenosine is required, then the number of possible m^{6}A sites in the MALAT1 triple helix is limited (Figure 1C). Another key consideration is how the binding of METTL16 alters the half-life of MALAT1 given that the triple helix functions as a stability element.[33] It is possible that the MALAT1 triple helix sponges METTL16 away from its methylation targets in the nucleus, but the physiological significance is not clear when the METTL16·MALAT1 triple helix is at a 1:1 stoichiometry (Figure 2C) and METTL16 is in vast excess over MALAT1 in both HeLa and HEK293T cells (>140-fold in both cell lines).[30,50] However, cellular concentration could potentially affect the dimerization potential of METTL16 because dimer formation appears more likely at higher concentrations of METTL16 based on previous size-exclusion chromatography and small-angle X-ray scattering results having METTL16 at 21 and 30 μM, respectively.[31] A possibility to consider is that METTL16 may be eliciting a methyltransferase-independent function when bound to MALAT1, as METTL16 enables translation and tumorigenesis in a manner independent of methylation and was recently found to inhibit MRE11, a DNA-end resection component, in an RNA-dependent manner.[51,52] The function of the METTL16·MALAT1 triple helix complex remains an enigma.

Given the differential interactions between METTL16 and various RNAs, METTL16 may exhibit unique kinetic mechanisms for each RNA substrate. For U6 snRNA, our preincubation and isotope partitioning assays support an ordered-sequential binding mechanism: METTL16 binds first to U6 snRNA and then SAM (Figure 5, Scheme 1). For the MAT2A hairpin, an X-ray crystal structure of METTL16·MAT2A hp1 suggests that SAM binds before RNA, whereas a solution-based preincubation methyltransferase assay supports a random-order binding mechanism.[25,40] The different substrate binding orders may depend on the RNA substrate. For instance, METTL16 requires the VCRs to bind tightly to U6 snRNA for efficient methylation, whereas methylation of MAT2A hp 1 does not require the VCRs.[26] Furthermore, U6 snRNA is proposed to undergo a conformational rearrangement, whereby a bend occurs at the region containing the UACAGAGAA motif while the VCRs stabilize the internal stem loop above the nonamer motif in the U6 snRNA (Figure 1B).[26] Such a conformational rearrangement by the VCRs does not impact the rate of methylation, but interestingly, the VCRs do enhance ternary complex formation (Figure 6, Table 1). Future studies are needed to further probe the rate-limiting steps for the k_{chem} and k_{cat} values. The K-loop, which appears to obstruct SAM binding in the solved structure of the METTL16·MAT2A hp1 complex, is one focal point because the structure could limit pre- or postchemistry steps.[25] Rate-limiting postchemistry steps could entail conformational changes of METTL16 or m^{6}A43 U6 snRNA, dissociation of m^{6}A43 U6 snRNA, or dissociation of *S*-adenosylhomocysteine (SAH). The relatively high K_{D3} of 1.1 μM for the m^{6}A43 U6 snRNA makes it tempting to speculate that m^{6}A43 U6 snRNA is not rate limiting; however, K_{D3} is a ratio of forward and reverse rate constants so those values will need to be measured to confirm.

Although METTL16 has only a few confirmed RNA substrates, METTL16 has a critical role in intracellular SAM regulation.[18] METTL16 along with cleavage factor Im components (CFI_m) 25, 59, and 68; the MAT2A hairpin 1; and other unidentified component(s) together function as a biosensor for SAM levels.[53] The intracellular concentrations of SAM for various mammalian cells are reported to be around 10 μM but can range from as low as 0.1 μM to as high as 1000 μM.[54] Accordingly, the K_{D2} of SAM interacting with the METTL16·U6 snRNA complex at 126 μM (Figure 6D, Table 1) reflects the role of METTL16 in regulating intracellular SAM concentrations.[18] In contrast, the K_D of the METTL3/METTL14·SAM complex is at 1.5 μM (Table 1); therefore, METTL3/METTL14 can maintain the m^{6}A status of its targets even under low intracellular SAM concentrations.[42] However, the METTL3/METTL14 complex exhibits K_D values of ∼10 μM for DRACH-containing RNA substrates while METTL16 achieves a K_D of 31 and 18 nM for the MALAT1 triple helix and U6 snRNA, respectively (Table 1).[42]

Under optimized buffer conditions, the catalytic efficiency of METTL16 with SAM under steady-state (k_{cat}/K_M) and pre-steady-state (k_{chem}/K_{D2}) conditions is 5.3×10^{-4} μM^{-1} min^{-1} and 4.4×10^{-3} μM^{-1} min^{-1}, respectively (Figure 6A−D, Table 1). Relative to the METTL3/METTL14 complex that exhibits a catalytic efficiency (k_{cat}/K_M) of 2.9 μM^{-1} min^{-1}, the catalytic efficiency of METTL3/METTL14 is much greater because of a 4-fold faster k_{cat} at 0.3 min^{-1} and a 1284-fold smaller K_M for SAM at 102 nM (Table 1).[43] In the literature, a wide range of k_{cat}/K_M values (SAM) have been measured for adenine-specific methyltransferases *in vitro*; however, METTL16 has an exceptionally poor catalytic efficiency due to its poor binding affinity for SAM and role in regulating intracellular SAM concentrations.[18] It is important to note that the poor catalytic efficiency of METTL16 is not due to the product SAH. Prior work showed that even 10-fold molar excess of SAH over SAM did not result in any observable inhibition of METTL16.[25]

Our results establish a basic kinetic scheme (Scheme 1) and parameters (Table 1) of METTL16 methylating U6 snRNA, a major RNA target.[17,18] This kinetic mechanism may vary for different RNA substrates, such as MAT2A hp 1 or those that lack the nonamer motif. Like the METTL16·MALAT1 triple helix complex, more unmethylated METTL16·RNA complexes may exist given the large RNA interactome of METTL16.[29] METTL16 represents an exciting drug target because of its methylation potential being tunable via SAM levels; therefore, it is theoretically possible to target hyper- and hypomethylation events observed in cancer. In summary, this study provides the

https://doi.org/10.1021/acs.biochem.2c00601
Biochemistry 2023, 62, 494−506

groundwork for understanding the kinetic mechanism of METTL16 in the context of its biological functions.

■ ASSOCIATED CONTENT

Supporting Information

The Supporting Information is available free of charge at https://pubs.acs.org/doi/10.1021/acs.biochem.2c00601.

Supplemental tables include sequences of DNA, RNA, and proteins used in this study; supplemental figures show results for various supporting biochemical and kinetic assays (PDF)

Accession Codes

METTL16, Uniprot ID Q86W50; METTL3, Uniprot ID Q86U44; METTL14, Uniprot ID Q9HCE5; TUTase, Uniprot ID Q9H6E5; MAT2A, Uniprot ID P31153; MRE11, Uniprot ID P49959

■ AUTHOR INFORMATION

Corresponding Author

Jessica A. Brown − *Department of Chemistry and Biochemistry, University of Notre Dame, Notre Dame, Indiana 46556, United States;* orcid.org/0000-0001-9055-5939; Email: jbrown33@nd.edu

Author

Kurtis Breger − *Department of Chemistry and Biochemistry, University of Notre Dame, Notre Dame, Indiana 46556, United States;* orcid.org/0000-0003-0066-4483

Complete contact information is available at: https://pubs.acs.org/10.1021/acs.biochem.2c00601

Author Contributions

Both authors have given approval to the final version of the manuscript. J.A.B. conceived and supervised the project. K.B. performed all experimentation except for assistance with the mass spectrometric instruments (refer to acknowledgments). K.B. and J.A.B. wrote the manuscript.

Funding

This work was funded by the Henry Luce Foundation, National Institutes of Health, National Institute of General Medical Sciences, and University of Notre Dame.

Notes

The authors declare no competing financial interest.

■ ACKNOWLEDGMENTS

We would like to give special thanks to Dr. Agnieszka Ruszkowska for preparing the full-length METTL16 and METTL16_291 plasmids, the Joan Steitz laboratory (Yale University) for sharing the HEK293T nuclear extract, the Biophysics Instrumentation Core for use of multiple instruments, the Warren Drug Discovery core facility for use of the microscale thermophoresis instrument, and the Mass Spectrometry & Proteomics Facility at Notre Dame for help with mass spectrometry experiments. We want to thank William Boggess and Mijoon Lee for providing advice and hands-on assistance with the mass spectrometry analyses. This study was supported by startup funds from the University of Notre Dame, the National Institutes of Health grants R00GM111430 and R35GM133696, and the Clare Boothe Luce Program of the Henry Luce Foundation. K.B. is a fellow of the Chemistry−Biochemistry−Biology Interface (CBBI) Program at the University of Notre Dame, supported by training grant T32GM075762 from the National Institute of General Medical Sciences. The content is solely the responsibility of the authors and does not necessarily represent the official views of the National Institute of General Medical Sciences nor the National Institutes of Health.

■ ABBREVIATIONS

ESI-MS, electrospray ionization mass spectrometry; hp, hairpin; *k*, rate constant; K_D, equilibrium dissociation constant; LC/ESI-MS/MS, liquid chromatography electrospray ionization tandem mass spectrometry; m^6A, N^6-methyladenosine; MALAT1, metastasis associated lung adenocarcinoma transcript 1; MAT2A, methionine adenosine transferase 2A transcript; METTL, methyltransferase-like protein; MST, microscale thermophoresis; SAH, *S*-adenosylhomocysteine; SAM, *S*-adenosylmethionine; TLC, thin layer chromatography; U6 snRNA, U6 small nuclear RNA; VCR, vertebrate conserved region

■ REFERENCES

(1) Linder, B.; Grozhik, A. V.; Olarerin-George, A. O.; Meydan, C.; Mason, C. E.; Jaffrey, S. R. Single-nucleotide-resolution mapping of m^6A and m^6Am throughout the transcriptome. *Nat. Methods* **2015**, *12*, 767−772.

(2) Koh, C. W. Q.; Goh, Y. T.; Goh, W. S. S. Atlas of quantitative single-base-resolution *N*6-methyl-adenine methylomes. *Nat. Commun.* **2019**, *10*, 5636.

(3) Meyer, K. D.; Saletore, Y.; Zumbo, P.; Elemento, O.; Mason, C. E.; Jaffrey, S. R. Comprehensive analysis of mRNA methylation reveals enrichment in 3′ UTRs and near stop codons. *Cell* **2012**, *149*, 1635−1646.

(4) Ries, R. J.; Zaccara, S.; Klein, P.; Olarerin-George, A.; Namkoong, S.; Pickering, B. F.; Patil, D. P.; Kwak, H.; Lee, J. H.; Jaffrey, S. R. m^6A enhances the phase separation potential of mRNA. *Nature* **2019**, *571*, 424−428.

(5) Yang, F.; Jin, H.; Que, B.; Chao, Y.; Zhang, H.; Ying, X.; Zhou, Z.; Yuan, Z.; Su, J.; Wu, B.; Zhang, W.; Qi, D.; Chen, D.; Min, W.; Lin, S.; Ji, W. Dynamic m^6A mRNA methylation reveals the role of METTL3-m^6A-CDCP1 signaling axis in chemical carcinogenesis. *Oncogene* **2019**, *38*, 4755−4772.

(6) Sabnis, R. W. Novel METTL3Modulators for Treating Acute Myeloid Leukemia (AML). *ACS Med. Chem. Lett.* **2021**, *12*, 1061−1062.

(7) Selberg, S.; Blokhina, D.; Aatonen, M.; Koivisto, P.; Siltanen, A.; Mervaala, E.; Kankuri, E.; Karelson, M. Discovery of small molecules that activate RNA methylation through cooperative binding to the METTL3−14-WTAP complex active site. *Cell Rep.* **2019**, *26*, 3762−3771.

(8) Littlefield, J. W.; Dunn, D. B. The occurrence and distribution of thymine and three methylated-adenine bases in ribonucleic acids from several sources. *Biochem. J.* **1958**, *70*, 642−651.

(9) Clancy, M. J.; Shambaugh, M. E.; Timpte, C. S.; Bokar, J. A. Induction of sporulation in *Saccharomyces cerevisiae* leads to the formation of *N*6-methyladenosine in mRNA: A potential mechanism for the activity of the IME4 gene. *Nucleic Acids Res.* **2002**, *30*, 4509−4518.

(10) Shen, L.; Liang, Z.; Wong, C. E.; Yu, H. Messenger RNA modifications in plants. *Trends Plant Sci.* **2019**, *24*, 328−341.

(11) Sergiev, P. V.; Serebryakova, M. V.; Bogdanov, A. A.; Dontsova, O. A. The YbiN gene of *Escherichia coli* encodes adenine-*N6* methyltransferase specific for modification of A1618 of 23 S ribosomal RNA, a methylated residue located close to the ribosomal exit tunnel. *J. Mol. Biol.* **2008**, *375*, 291−300.

(12) Dominissini, D.; Moshitch-Moshkovitz, S.; Schwartz, S.; Salmon-Divon, M.; Ungar, L.; Osenberg, S.; Cesarkas, K.; Jacob-Hirsch, J.; Amariglio, N.; Kupiec, M.; Sorek, R.; Rechavi, G. Topology

of the human and mouse m^{6}A RNA methylomes revealed by m^{6}A-seq. *Nature* **2012**, *485*, 201−206.
(13) Nachtergaele, S.; He, C. Chemical modifications in the life of an mRNA transcript. *Annu. Rev. Genet.* **2018**, *52*, 349−372.
(14) Fazi, F.; Fatica, A. Interplay between *N*6-methyladenosine (m^{6}A) and noncoding RNAs in cell development and cancer. *Front. Cell Dev. Biol.* **2019**, *7*, 116.
(15) Ma, H.; Wang, X.; Cai, J.; Dai, Q.; Natchiar, S. K.; Lv, R.; Chen, K.; Lu, Z.; Chen, H.; Shi, Y. G. Y.; Lan, F.; Fan, J.; Klaholz, B. P.; Pan, T.; Shi, Y. G. Y.; He, C. *N*6-methyladenosine methyltransferase ZCCHC4 mediates ribosomal RNA methylation. *Nat. Chem. Biol.* **2019**, *15*, 88−94.
(16) Piekna-Przybylska, D. D.; Decatur, W. A.; Fournier, M. J. The 3D rRNA modification maps database: With interactive tools for ribosome Analysis. *Nucleic Acids Res.* **2007**, *36*, D178−D183.
(17) Shimba, S.; Bokar, J. A.; Rottman, F.; Reddy, R. Accurate and efficient *N*-6-adenosine methylation in spliceosomal U6 small nuclear RNA by HeLa cell extract *in vitro*. *Nucleic Acids Res.* **1995**, *23* (13), 2421−2426.
(18) Pendleton, K. E.; Chen, B.; Liu, K.; Hunter, O. V.; Xie, Y.; Tu, B. P.; Conrad, N. K. The U6 snRNA m^{6}A methyltransferase METTL16 regulates SAM synthetase intron retention. *Cell* **2017**, *169*, 824−835.
(19) Saneyoshi, M.; Harada, F.; Nishimura, S. Isolation and characterization of *N*6-methyladenosine from *Escherichia coli* valine transfer RNA. *BBA Sect. Nucleic Acids Protein Synth.* **1969**, *190*, 264−273.
(20) Wang, X.; Lu, Z.; Gomez, A.; Hon, G. C.; Yue, Y.; Han, D.; Fu, Y.; Parisien, M.; Dai, Q.; Jia, G.; Ren, B.; Pan, T.; He, C. *N*6-methyladenosine-dependent regulation of messenger RNA stability. *Nature* **2014**, *505*, 117−120.
(21) Meyer, K. D.; Patil, D. P.; Zhou, J.; Zinoviev, A.; Skabkin, M. A.; Elemento, O.; Pestova, T. V.; Qian, S. B.; Jaffrey, S. R. 5′ UTR m^{6}A Promotes Cap-Independent Translation. *Cell* **2015**, *163*, 999−1010.
(22) Van Tran, N.; Ernst, F. G. M.; Hawley, B. R.; Zorbas, C.; Ulryck, N.; Hackert, P.; Bohnsack, K. E.; Bohnsack, M. T.; Jaffrey, S. R.; Graille, M.; Lafontaine, D. L. J. The human 18S rRNA m^{6}A methyltransferase METTL5 is stabilized by TRMT112. *Nucleic Acids Res.* **2019**, *47*, 7719−7733.
(23) Liu, J.; Yue, Y.; Han, D.; Wang, X.; Fu, Y.; Zhang, L.; Jia, G.; Yu, M.; Lu, Z.; Deng, X.; Dai, Q.; Chen, W.; He, C. A METTL3-METTL14 complex mediates mammalian nuclear RNA *N*6-adenosine methylation. *Nat. Chem. Biol.* **2014**, *10*, 93−95.
(24) Mendel, M.; Chen, K. M.; Homolka, D.; Gos, P.; Pandey, R. R.; McCarthy, A. A.; Pillai, R. S. Methylation of structured RNA by the m^{6}A writer METTL16 is essential for mouse embryonic development. Mol. *Cell* **2018**, *71*, 986−1000.
(25) Doxtader, K. A.; Wang, P.; Scarborough, A. M.; Seo, D.; Conrad, N. K.; Nam, Y. Structural basis for regulation of METTL16, an *S*-adenosylmethionine homeostasis Factor. *Mol. Cell* **2018**, *71*, 1001−1011.e4.
(26) Aoyama, T.; Yamashita, S.; Tomita, K. Mechanistic insights into m^{6}A modification of U6 snRNA by human METTL16. *Nucleic Acids Res.* **2020**, *48*, 5157−5168.
(27) Ishigami, Y.; Ohira, T.; Isokawa, Y.; Suzuki, Y.; Suzuki, T. A single m^{6}A modification in U6 snRNA diversifies exon sequence at the 5′ splice site. *Nat. Commun.* **2021**, *12*, 3244.
(28) Shima, H.; Matsumoto, M.; Ishigami, Y.; Ebina, M.; Muto, A.; Sato, Y.; Kumagai, S.; Ochiai, K.; Suzuki, T.; Igarashi, K. *S*-Adenosylmethionine synthesis is regulated by selective *N*6-adenosine methylation and mRNA degradation involving METTL16 and YTHDC1. *Cell Rep.* **2017**, *21*, 3354−3363.
(29) Warda, A. S.; Kretschmer, J.; Hackert, P.; Lenz, C.; Urlaub, H.; Höbartner, C.; Sloan, K. E.; Bohnsack, M. T. Human METTL16 is a *N*^{6}-methyladenosine (m^{6}A) methyltransferase that targets pre-mRNAs and various non-coding RNAs. *EMBO Rep.* **2017**, *18*, 2004−2014.
(30) Brown, J. A.; Kinzig, C. G.; Degregorio, S. J.; Steitz, J. A. Methyltransferase-like protein 16 binds the 3′-terminal triple helix of MALAT1 long noncoding RNA. *Proc. Natl. Acad. Sci.USA* **2016**, *113*, 14013−14018.
(31) Ruszkowska, A.; Ruszkowski, M.; Dauter, Z.; Brown, J. A. Structural insights into the RNA methyltransferase domain of METTL16. *Sci. Rep.* **2018**, *8*, 5311.
(32) Kim, Y.; Babnigg, G.; Jedrzejczak, R.; Eschenfeldt, W. H.; Li, H.; Maltseva, N.; Hatzos-Skintges, C.; Gu, M.; Makowska-Grzyska, M.; Wu, R.; An, H.; Chhor, G.; Joachimiak, A. High-throughput protein purification and quality assessment for crystallization. *Methods.* **2011**, *55*, 12−28.
(33) Brown, J. A.; Bulkley, D.; Wang, J.; Valenstein, M. L.; Yario, T. A.; Steitz, T. A.; Steitz, J. A. Structural insights into the stabilization of MALAT1 noncoding RNA by a bipartite triple helix. *Nat. Struct. Mol. Biol.* **2014**, *21*, 633−640.
(34) Brown, J. A.; Valenstein, M. L.; Yario, T. A.; Tycowski, K. T.; Steitz, J. A. Formation of triple-helical structures by the 3′-end sequences of MALAT1 and MENβ noncoding RNAs. *Proc. Natl. Acad. Sci. U.S.A.* **2012**, *109*, 19202−19207.
(35) Kershaw, C. J.; O'Keefe, R. T. Splint ligation of RNA with T4 DNA ligase. *Methods Mol. Biol.* **2013**, *941*, 257−269.
(36) Jerabek-Willemsen, M.; André, T.; Wanner, R.; Roth, H. M.; Duhr, S.; Baaske, P.; Breitsprecher, D. Microscale thermophoresis: Interaction analysis and beyond. *J. Mol. Struct.* **2014**, *1077*, 101−113.
(37) Yuan, B. F. Liquid chromatography-mass spectrometry for analysis of RNA adenosine methylation. *Methods Mol. Biol.* **2017**, *1562*, 33−42.
(38) Hou, Y. M. Single-turnover kinetics of methyl transfer to tRNA by methyltransferases. *Methods Mol. Biol.* **2016**, *1421*, 79−96.
(39) Gasteiger, E.; Gattiker, A.; Hoogland, C.; Ivanyi, I.; Appel, R. D.; Bairoch, A. ExPASy: The proteomics server for in-depth protein knowledge and analysis. *Nucleic Acids Res.* **2003**, *31*, 3784−3788.
(40) Yu, D.; Kaur, G.; Blumenthal, R. M.; Zhang, X.; Cheng, X. Enzymatic characterization of three human RNA adenosine methyltransferases reveals diverse substrate affinities and reaction optima. *J. Biol. Chem.* **2021**, *296*, 100270.
(41) Reich, N. O.; Mashhoon, N. Presteady state kinetics of an *S*-adenosylmethionine-dependent enzyme. Evidence for a unique binding orientation requirement for *Eco*RI DNA methyltransferase. *J. Biol. Chem.* **1993**, *268*, 9191−9193.
(42) Wang, X.; Feng, J.; Xue, Y.; Guan, Z.; Zhang, D.; Liu, Z.; Gong, Z.; Wang, Q.; Huang, J.; Tang, C.; Zou, T.; Yin, P. Structural Basis of N6-Adenosine Methylation by the METTL3-METTL14 Complex. *Nature* **2016**, *534*, 575−578.
(43) Li, F.; Kennedy, S.; Hajian, T.; Gibson, E.; Seitova, A.; Xu, C.; Arrowsmith, C. H.; Vedadi, M. A. A radioactivity-based assay for screening human m^{6}A-RNA methyltransferase, METTL3-METTL14 complex, and demethylase ALKBH5. *J. Biomol. Screen.* **2016**, *21*, 290−297.
(44) Csepany, T.; Lin, A.; Baldick, C. J.; Beemon, K. Sequence specificity of mRNA *N*6-adenosine methyltransferase. *J. Biol. Chem.* **1990**, *265*, 20117−20122.
(45) Dominissini, D.; Moshitch-Moshkovitz, S.; Salmon-Divon, M.; Amariglio, N.; Rechavi, G. Transcriptome-wide mapping of *N*^{6}-Methyladenosine by m^{6}A-seq based on immunocapturing and massively parallel sequencing. *Nat. Protoc.* **2013**, *8*, 176−189.
(46) Wei, C. M.; Moss, B. Nucleotide sequences at the *N*^{6}-Methyladenosine Sites of HeLa Cell Messenger Ribonucleic Acid. *Biochemistry* **1977**, *16*, 1672−1676.
(47) Narayan, P.; Rottman, F. M. An *in vitro* system for accurate methylation of internal adenosine residues in messenger RNA. *Science* **1988**, *242*, 1159−1162.
(48) Harper, J. E.; Miceli, S. M.; Roberts, R. J.; Manley, J. L. Sequence specificity of the human mRNA N6-Adenosine Methylase *in vitro*. *Nucleic Acids Res.* **1990**, *18*, 5735−5741.
(49) Wilusz, J. E.; Freier, S. M.; Spector, D. L. 3′ end processing of a long nuclear-retained noncoding RNA yields a tRNA-like cytoplasmic RNA. *Cell* **2008**, *135*, 919−932.

https://doi.org/10.1021/acs.biochem.2c00601
Biochemistry 2023, 62, 494−506

(50) Tripathi, V.; Ellis, J. D.; Shen, Z.; Song, D. Y.; Pan, Q.; Watt, A. T.; Freier, S. M.; Bennett, C. F.; Sharma, A.; Bubulya, P. A.; Blencowe, B. J.; Prasanth, S. G.; Prasanth, K. V. The nuclear-retained noncoding RNA MALAT1 regulates alternative splicing by modulating SR splicing factor phosphorylation. *Mol. Cell* **2010**, *39*, 925−938.
(51) Su, R.; Dong, L.; Li, Y.; Gao, M.; He, P. C.; Liu, W.; Wei, J.; Zhao, Z.; Gao, L.; Han, L.; Deng, X.; Li, C.; Prince, E.; Tan, B.; Qing, Y.; Qin, X.; Shen, C.; Xue, M.; Zhou, K.; Chen, Z.; Xue, J.; Li, W.; Qin, H.; Wu, X.; Sun, M.; Nam, Y.; Chen, C. W.; Huang, W.; Horne, D.; Rosen, S. T.; He, C.; Chen, J. METTL16 exerts an m^6A-independent function to facilitate translation and tumorigenesis. *Nat. Cell Biol.* **2022**, *24*, 205−216.
(52) Zeng, X.; Zhao, F.; Cui, G.; Zhang, Y.; Deshpande, R. A.; Chen, Y.; Deng, M.; Kloeber, J. A.; Shi, Y.; Zhou, Q.; Zhang, C.; Hou, J.; Kim, W.; Tu, X.; Yan, Y.; Xu, Z.; Chen, L.; Gao, H.; Guo, G.; Liu, J.; Zhu, Q.; Cao, Y.; Huang, J.; Wu, Z.; Zhu, S.; Yin, P.; Luo, K.; Mer, G.; Paull, T. T.; Yuan, J.; Tao, K.; Lou, Z. METTL16 antagonizes MRE11-mediated DNA end resection and confers synthetic lethality to PARP inhibition in pancreatic ductal adenocarcinoma. *Nat. Cancer* **2022**, *3*, 1088−1104.
(53) Scarborough, A. M.; Flaherty, J. N.; Hunter, O. V.; Liu, K.; Kumar, A.; Xing, C.; Tu, B. P.; Conrad, N. K. SAM homeostasis is regulated by CFI_m-mediated splicing of MAT2A. *Elife* **2021**, *10*, e64930.
(54) Ye, C.; Tu, B. P. Sink into the epigenome: Histones as repositories that influence cellular metabolism. *Trends Endocrinol Metab.* **2018**, *29*, 626−637.

https://doi.org/10.1021/acs.biochem.2c00601
Biochemistry 2023, 62, 494−506